

## Supporting Information

### **Aggregation-induced emission (AIE)-active molecules bearing singlet oxygen generation activities: the tunable singlet-triplet energy gap matters**

**Chengkai Zhang<sup>†a,b</sup>, Yanqian Zhao<sup>†a,b</sup>, Dandan Li<sup>\*a</sup>, Jiejie Liu<sup>c</sup>, Heguo Han<sup>b</sup>, Daoyu He<sup>b</sup>, Xiaohe Tian<sup>c</sup>, Shengli Li<sup>b</sup>, Jieying Wu<sup>b</sup>, Yupeng Tian<sup>\*b</sup>**

<sup>a</sup>Institute of Physics Science and Information Technology, Anhui University, Hefei 230601, China

<sup>b</sup>Department of Chemistry, Key Laboratory of Functional Inorganic Material Chemistry of Anhui Province, Anhui University, Hefei 230601, P. R. China

<sup>c</sup>School of Life Science, Anhui University, Hefei 230601, P. R. China

<sup>†</sup>These authors contributed equally to this work.

\*Corresponding author: chemlidd@163.com; yptian@ahu.edu.cn

1.1. Materials and Apparatus.....	2
1.2. Computational details.....	2
1.3. Two-photon excited fluorescence (TPEF) spectroscopy.....	3
1.4. SEM experiment.....	3
1.5. Cytotoxicity assays in cells .....	4
1.6. Singlet oxygen ( <sup>1</sup> O <sub>2</sub> ) detection.....	4
1.7. X-ray crystallography.....	5
1.8. Synthesis.....	5
1.9. Results and disscussion.....	7
Notes and references.....	19

## Experimental Section

### 1.1 Materials and Apparatus

All chemicals and solvents were dried and purified by usual methods. The synthetic routes for the compounds and their derivatives were illustrated in **Scheme. S1**. Both the compounds were purified over recrystallization. The <sup>1</sup>H-NMR and <sup>13</sup>C-NMR spectra recorded on at 25°C, using Bruker 400/600 Ultrashield spectrometer were reported as parts per million (ppm) from TMS (δ). IR spectra were recorded on a Nicolet FTIR-instrument (mid-IR: 4000 ~ 400 cm<sup>-1</sup> range with KBr discs; Far-IR: 600-50 cm<sup>-1</sup>, using a powder sample on a PE film attached with paroline). MALDI-TOF mass spectra were recorded using Bruker Autoflex III Smartbeam. ESI Mass Spectrometer was recorded using LCQ Fleet. UV-vis absorption spectra were recorded on a UV-265 spectrophotometer. Fluorescence measurements were carried out on a Hitachi F-7000 fluorescence spectrophotometer.

### 1.2. Computational details

To better understand the charge transfer state, time-dependent density functional theory (TD-DFT) calculations on all the compounds were carried out in THF. Optimizations were carried out with B3LYP functional without any symmetry restraint, and the TD-DFT calculations were performed on the optimized structure with B3LYP functional. All calculations, including optimizations and TD-DFT, were performed

with the G09 software. Geometry optimization of the singlet ground state and the TD-DFT calculation of the lowest 25 singlet–singlet excitation energies were calculated with a basis set composed of 6-31 G\* for C H N O P F atoms. An analytical frequency confirms evidence that the calculated species represents a true minimum without imaginary frequencies on the respective potential energy surface. The lowest 25 spin-allowed singlet-singlet transitions, up to energy of about 5 eV were taken into account in the calculation of the absorption spectra.

### 1.3. Two-photon excited fluorescence (TPEF) spectroscopy

Two-photon cross-sections of the compounds were recorded using two-photon excited fluorescence measurements with a femtosecond laser pulse, to avoid the possibility of excited state absorption, and a Ti: sapphire system (690-1080 nm, 80 MHz, 140 fs) as the light source. The 2PA cross section ( $\sigma$ ) was determined by comparing their TPEF to that of fluorescein, according to the following equation:

$$\sigma_s = \frac{\sigma_r \times F_s \times C_r \times n_r}{F_r \times \Phi_s \times C_s \times n_s}$$

where the subscripts ‘‘s’’ and ‘‘r’’ represent sample and reference (here, fluorescein in an NaOH solution was used as reference and samples were all in concentration of  $2.0 \times 10^{-4}$  mol/L with a 1 cm standard quartz cell). F is the two-photon excited fluorescence integral intensity of the solution emitted at the exciting wavelength.  $\Phi$ , n and c are the quantum yield of the fluorescence, the refractive index of the solvent, and the concentration of the solution, respectively. The values of  $\sigma_r$  at different wavelengths and  $\Phi_r$  are taken from the literature.

### 1.4. SEM experiment

SEM samples were sectioned in Araldite resin by microtome and examined on a FEI Tecnai instrument operating at 80 kV equipped with a Gatan 1 k CCD Camera.

### 1.5. Cytotoxicity assays in cells

The study of the effect of **L2b NPs** and **L2c NPs** on viability of cells was carried out using the methylthiazolyldiphenyl-tetrazolium bromide (MTT) assay. **L2b NPs** or

**L2c NPs** stock solutions were diluted by fresh medium in to desired concentration (2, 4, 6, 8, 10, 12  $\mu\text{M}$ ). HeLa cells were cultured in a 96-well plate for 24 h before experiments. The cell medium was then exchanged by different concentrations of **L2b NPs** or **L2c NPs** medium solutions. They were then incubated at 37 °C in 5%  $\text{CO}_2$  for 24 h before cell viability was measured by the MTT assay. The cell medium solutions were exchanged by 100  $\mu\text{L}$  of fresh medium, followed by the addition of 20  $\mu\text{L}$  (5 mg/mL) MTT solution to each well. The cell plates were then incubated at 37 °C in 5%  $\text{CO}_2$  for 4 h. Absorbance was measured at 490 nm. The absorbance measured for an untreated cell population under the same experimental conditions was used as the reference point to establish 100% cell viability. Duplicated experiments have been tested. MTT assay to assess the in vitro PDT efficacy of **L2b NPs** and **L2c NPs** was performed under 808 nm laser irradiation.

### 1.6. Singlet oxygen ( $^1\text{O}_2$ ) detection

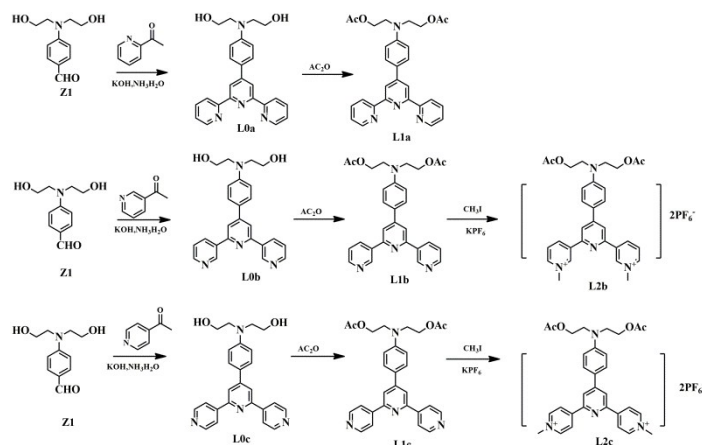
In this study, the amount of singlet oxygen was detected by a singlet oxygen sensor named 9,10-anthracene-dipropionic acid disodium salt (ADPA), because the newly generated singlet oxygen could cause an absorbance decrease of the chemical probe at around 400 nm. Briefly, 3 mL of micelles solution was mixed with 15 mL of ADPA solution (15 mM) and then exposed to laser excitation at 808 nm for 1, 2, 5, 10 min (808 nm laser beam was purchased from Xian Midriver Optoelectronics Technology Co., Ltd, China.). The absorbance of the probe was measured at the same time-scale to evaluate the generation of singlet oxygen in different samples.

### 1.7. X-ray crystallography

Single-crystal X-ray diffraction measurements were carried out on a Bruker Smart 1000 CCD diffractometer equipped with a graphite crystal monochromator situated in the incident beam for data collection at room temperature. The determination of unit cell parameters and data collections were performed with  $\text{Mo-K}_\alpha$  radiation ( $\lambda=0.71073$  Å). Unit cell dimensions were obtained with least-squares refinements, and all structures were solved by direct methods using SHELXL-97 program package. All non-

hydrogen atoms were refined anisotropically. The hydrogen atoms were added theoretically and riding on the concerned atoms. The final refinement was performed by full-matrix least-squares methods with anisotropic thermal parameters for non-hydrogen atoms on F<sup>2</sup>.

## 1.8. Synthesis



**Scheme S1** Synthetic procedures for target molecules **L1-L2**.

(1) **Synthesis of L0a:** Z1 4.2 g (0.02 mol) was dissolved completely in 250 mL ethanol solution, then 2-acetyl pyridine 4.9 g (0.041 mol) was added successively, 20 mL ammonia (25 %) and potassium hydroxide 3.0 g (0.05 mol) were added in turn. The reaction was stirred at 80 °C for 4 h. The bottom of the flask with a large number of solid precipitation, and filter after cooling, yellow product was obtain, yield 50 %. <sup>1</sup>H NMR δ (ppm): 8.77 (t, 2H), 8.64 (t, 4H), 8.02 (t, 2H), 7.76 (d, 2H), 7.52 (t, 2H), 6.89 (d, 2H), 4.85 (t, 2H), 3.59 (q, 8H). <sup>13</sup>C NMR (100 MHz, DMSO-d<sub>6</sub>) δ (ppm): 155.91, 155.37, 152.09, 150.01, 149.19, 137.22, 123.61, 128.30, 121.38, 118.04, 112.73, 61.73, 58.90. ESI-MS: calculated for [M+H]<sup>+</sup>: 413.48, *found*: 413.6.

(2) **Synthesis of L0b, L0c:** The synthesis of compounds is similar to that of L0a, with Z1 respectively in the reaction of 3-acetylpyridine and 4-acetylpyridine, treatment and separation are the same as L0a.

**L0b:** <sup>1</sup>H NMR: δ(ppm) 8.67 (t, 4H), 8.25 (s, 2H), 7.94 (d, 2H), 7.56 (t, 2H), 6.84 (d, 2H), 4.79 (t, 2H), 3.60 (t, 4H), 3.52 (t, 4H). <sup>13</sup>C NMR (100 MHz, DMSO-d<sub>6</sub>) δ (ppm): 152.81, 151.37, 150.10, 149.51, 148.81, 134.62, 134.53, 128.31, 124.10, 116.62, 112.7,

61.73, 58.93. ESI-MS: calculated for  $[M+H]^+$ : 413.48, *found*: 413.6.

**L0c:**  $^1\text{H}$ NMR:  $\delta$ (ppm) 8.76 (d, 2H), 8.36 (s, 2H), 8.32 (d, 4H), 7.96 (d, 2H), 6.86 (d, 2H), 4.81 (t, 2H), 3.62 (q, 4H), 3.54 (t, 4H).  $^{13}\text{C}$  NMR (100 MHz, DMSO- $d_6$ )  $\delta$  (ppm): 153.61, 152.01, 150.10 149.81, 145.71, 131.82, 128.33, 121.41, 115.60, 112.72, 61.73, 58.93. ESI-MS: calculated for  $[M+H]^+$ : 413.48, *found*:413.6.

**(3) Synthesis of L1a:** L0a 2.06 g (0.005 mol) was dissolved completely in 8 mL pyridine, then 2 mL (20 mmol) acetic anhydride was added successively. The reaction was stirred at 110°C for 4 h. The mixture was cooled to room temperature After reaction stops. Extracting by  $\text{CH}_2\text{Cl}_2$ , and then concentrated removing solvent to crude product. Purified by column chromatography (petroleum ether: ethanol = 5:1), obtaining product 1.98 g. yield 79.9 %.  $^1\text{H}$  NMR (400 MHz, DMSO- $d_6$ )  $\delta$  (ppm): 8.77 (d, 2H, J = 8.0 Hz), 8.66 (m, 4H, J = 8.2 Hz), 8.03 (t, 2H, J = 7.8 Hz), 7.79 (d, 2H, J = 8.8 Hz), 7.52 (ddd, 2H, J = 7.6, 4.8, 1.2 Hz), 6.97 (d, 2H, J = 8.8 Hz), 4.23 (t, 4H, J = 6.0 Hz), 3.70 (t, 4H, J = 5.8 Hz), 2.03 (s, 6H).  $^{13}\text{C}$  NMR (100 MHz, DMSO- $d_6$ )  $\delta$  (ppm): 170.37, 155.37, 155.20, 149.23, 149.09, 148.52, 137.38, 127.70, 124.34, 120.86, 116.38, 112.25, 61.00, 48.86, 20.65. ESI-MS: calculated for  $[M+H]^+$ : 497.22, *found* 497.22.

**(4) Synthesis of L1b, L1c:** The synthesis of ligands is similar to that of **L1a**.

**L1b:**  $^1\text{H}$  NMR (400 MHz, DMSO- $d_6$ )  $\delta$  (ppm): 9.50 (s, 2H), 8.68 (d, 4H, J = 5.6 Hz), 8.29 (s, 2H, J = 8.3 Hz), 8.01 (d, 2H, J = 8.8 Hz), 7.57 (m, 2H), 6.95 (d, 2H, J = 8.8 Hz), 4.22 (t, 4H, J = 6.0 Hz), 3.71 (t, 4H, J = 6.1 Hz), 2.02 (s, 6H, J = 6.8 Hz).  $^{13}\text{C}$  NMR (100 MHz, DMSO- $d_6$ )  $\delta$  (ppm): 170.39, 154.37, 149.86, 149.61, 148.56, 148.13, 134.41, 134.28, 128.36, 124.08, 123.71, 115.90, 111.96, 60.95, 48.87, 20.65. ESI-MS: calculated for  $[M+H]^+$  497.22, *found* 497.22.

**L1c:**  $^1\text{H}$  NMR (400 MHz, DMSO- $d_6$ )  $\delta$  (ppm): 9.50 (s, 2H), 8.68 (d, 4H, J = 5.6 Hz), 8.29 (s, 2H, J = 6.8 Hz), 8.01 (d, 2H, J = 8.8 Hz), 7.57 (m, 2H, J = 7.6 Hz), 6.95 (d, 2H, J = 8.8 Hz), 4.22 (t, 4H, J = 6.0 Hz), 3.71 (t, 4H, J = 6.1 Hz), 2.02 (s, 6H, J = 6.9 Hz).  $^{13}\text{C}$  NMR (100 MHz, DMSO- $d_6$ )  $\delta$  (ppm): 170.39, 154.37, 149.86, 149.61, 148.56, 148.13, 134.41, 134.28, 128.36, 124.08, 123.71, 115.90, 111.96, 60.95, 48.87, 20.65. ESI-MS: calculated for  $[M+H]^+$ : 497.22, *found* 497.22.

**(5) Synthesis of L2b:** L1b (1 g, 2 mmol) was dissolved at 10 mL methanol, then

methyl iodide (1.5 g, 10 mmol) was added successively. The reaction was stirred at 43 °C for 24 h, then Potassium hexafluorophosphate was added successively. The mixture was cooled to room temperature and washed at normal hexane. Filtering off and obtain yellow product 1.47 g, yield 74 %. <sup>1</sup>H NMR (600 MHz, CD<sub>3</sub>CN) δ 9.63 (s, 2H), 9.35 (d, *J* = 8.2 Hz, 2H), 8.74 (d, *J* = 5.9 Hz, 2H), 8.41 (s, 2H), 8.2 (m, *J* = 8.7 Hz, 2H), 7.96 (d, *J* = 8.7 Hz, 2H), 7.06 (d, *J* = 8.7 Hz, 2H), 4.50 (s, 6H), 4.30 (t, *J* = 6.0 Hz, 4H), 3.77 (d, *J* = 6.1 Hz, 4H), 2.03 (s, 6H). <sup>13</sup>C-NMR (100 MHz, CD<sub>3</sub>CN, ppm): δ 20.09, 48.70, 49.29, 60.93, 112.40, 117.34, 118.86, 127.99, 128.51, 138.51, 142.76, 144.29, 145.09, 150.80, 151.75. ESI-MS: calculated for [M<sup>+</sup>]: 526.26, *found* 526.26.

**(6) Synthesis of L2c:** L1c (1 g, 2 mmol) was added into 250 mL flask, then methyl iodide (1.5 g, 10 mmol) was added successively. The reaction was stirred at 43 °C for 24 h, then Potassium hexafluorophosphate was added successively. The mixture was cooled to room temperature and washed at normal hexane. Filtering off and obtain yellow product 1.31 g, yield 65 %. <sup>1</sup>H NMR (600 MHz, CD<sub>3</sub>CN) δ 8.89 (d, *J* = 6.3 Hz, 4H), 8.80 (d, *J* = 6.3 Hz, 4H), 8.58 (s, 2H), 7.97 (d, *J* = 8.7 Hz, 2H), 7.06 (d, *J* = 8.7 Hz, 2H), 4.39 (s, 6H), 4.30 (t, *J* = 6.0 Hz, 4H), 3.76 (t, *J* = 6.1 Hz, 4H), 2.03 (s, 6H). <sup>13</sup>C NMR (100 MHz, CD<sub>3</sub>CN) δ 170.80, 153.30, 152.25, 151.22, 149.77, 145.72, 128.65, 125.10, 121.40, 117.39, 112.38, 60.97, 49.27, 47.91, 20.09. ESI-MS: calculated for [M<sup>+</sup>]: 526.26, *found*: 526.26.

## 1.9. Results and discussion

### (1) AIE mechanism

Indeed, the restriction of the intramolecular rotation (RIR) process has been proposed to be the main cause for classic AIE system, which is the working mechanism for our work as well.

Firstly, molecular packing of **L2b** and **L2c** (shown in Scheme 1c) indicated that C-H... $\pi$  hydrogen bonds are formed between the hydrogen atoms in the phenyl rings of one molecule and the  $\pi$  electrons of the phenyl rings of another adjacent molecule. Such interactions could assist in locking the molecular motion and reducing the nonradiative deactivation of excitons, *ie.*, favoring RIR process.<sup>S1-S4</sup>

Secondly, massive hydrogen-bonding interactions existed between two adjacent molecules (shown in Scheme 1c). These noncovalent interactions helped to hold the molecules together and rigidify their molecular structures, activating the RIR process.<sup>S1,S5</sup>

Benefiting from the RIR process, **L2b NPs** and **L2c NPs** exhibited excellent AIE behavior. As shown in **Table S1**, the fluorescence quantum yields (QY) of **L2b** and **L2c** in aqueous solution have been measured by using an integrating sphere on FLSP920. In addition, the fluorescence quantum yields of **L2b NPs** and **L2c NPs** in aqueous solution have been measured as well, which show significant enhancement due to the AIE behavior.

## (2) Singlet oxygen quantum yield

**L2b** and **L2c** are nearly non-emissive in the molecularly dissolved state, which showed very low <sup>1</sup>O<sub>2</sub> generation ability owing to the consumption of excitonic energy by free intramolecular motions.<sup>S6</sup> In contrast to this, **L2b** and **L2c** become highly emissive upon aggregation caused by the restriction of intramolecular rotations (RIR), which block the nonradiative pathway and activate the radiative channels for energy dissipation,<sup>S1</sup> resulting in higher <sup>1</sup>O<sub>2</sub> generation ability upon loading into nanocarriers (*ie.* **L2b NPs** and **L2c NPs**).<sup>S6-S8</sup> Furthermore, compared with the solution-state (Figure 1c), **L2b** and **L2c** upon aggregation exhibit obviously long-lived excited states (10.11 ms and 10.81 ms, respectively, Figure 1d), which is beneficial to ISC process favoring the <sup>1</sup>O<sub>2</sub> generation.

To assess the capabilities of **L2b NPs** and **L2c NPs** for <sup>1</sup>O<sub>2</sub> generation, a commercial <sup>1</sup>O<sub>2</sub> probe, 9,10-anthracene-dipropionic acid disodium salt (ADPA), was used as an indicator, and Rose Bengal (RB) was employed as the standard photosensitizer (the <sup>1</sup>O<sub>2</sub> quantum yield for RB is 0.75 in water). As shown in Fig. S14, under 808 nm light irradiation, the presence of **L2b NPs**, **L2c NPs** or RB leads to gradually decreased ADPA absorbance with prolonged irradiation time, indicating degradation of ADPA by the generated <sup>1</sup>O<sub>2</sub> in solution. According to calculation formula for singlet oxygen yield, the <sup>1</sup>O<sub>2</sub> quantum yields of **L2b NPs** and **L2c NPs** were 0.401 and 0.355, respectively.

The details of  $^1\text{O}_2$  quantum yield measurements are listed as follows:

The  $^1\text{O}_2$ -sensitive indicator 9,10-anthracene-dipropionic acid disodium salt (ADPA) was used as the  $^1\text{O}_2$  indicator, and Rose Bengal (RB) was employed as the standard photosensitizer. In these experiments, 15 mL of ADPA solution (15 mM) was added to 3 mL of micelles solution, and 808 nm light with a power density of  $500 \text{ mW cm}^{-2}$  was used as the irradiation source. The absorbance of ADPA at 808 nm was recorded at different irradiation times to obtain the decay rate of the photosensitizing process. The  $^1\text{O}_2$  quantum yield of the PS in water ( $\phi_{\text{PS}}$ ) was calculated using the following formula:

$$\Phi_{\text{PS}} = \Phi_{\text{RB}} \frac{K_{\text{PS}} A_{\text{RB}}}{K_{\text{RB}} A_{\text{PS}}},$$

where  $K_{\text{PS}}$  and  $K_{\text{RB}}$  are the decomposition rate constants of ADPA by the PSs and RB, respectively.  $A_{\text{PS}}$  and  $A_{\text{RB}}$  represent the light absorbed by the PSs and RB, respectively, which are determined by integration of the areas under the absorption bands in the wavelength range of 400–800 nm.  $\phi_{\text{RB}}$  is the  $^1\text{O}_2$  quantum yield of RB, which is 0.75 in water.

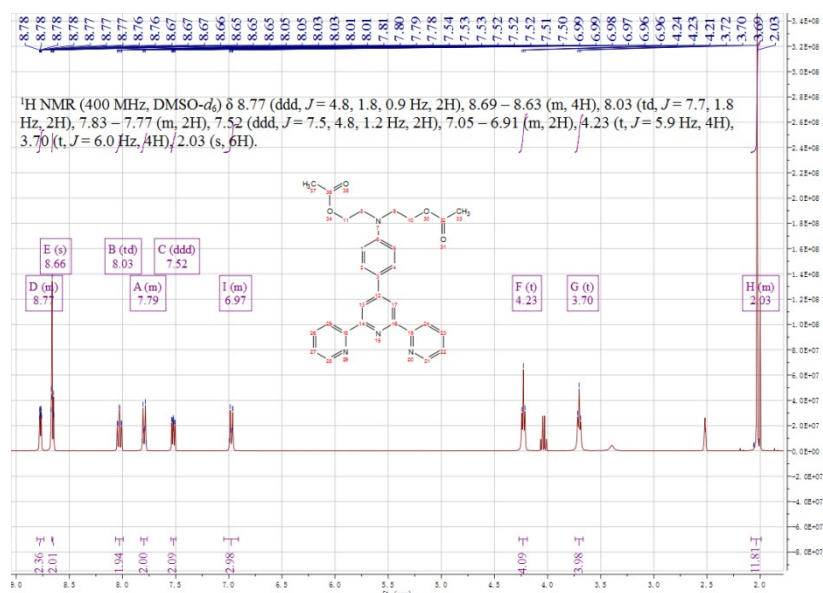


**Fig. S1**  $^1\text{H}$ -NMR spectrum of L1a.

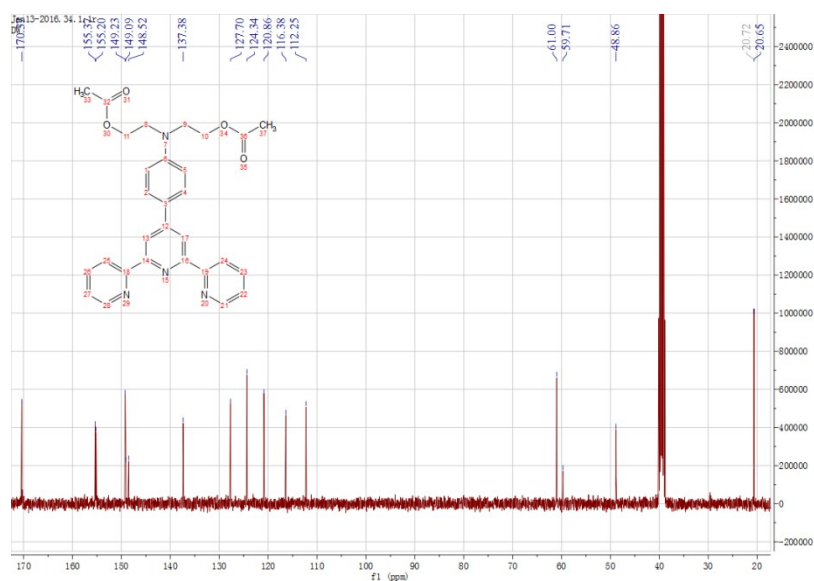


Fig. S2  $^{13}\text{C-NMR}$  spectrum of L1a.

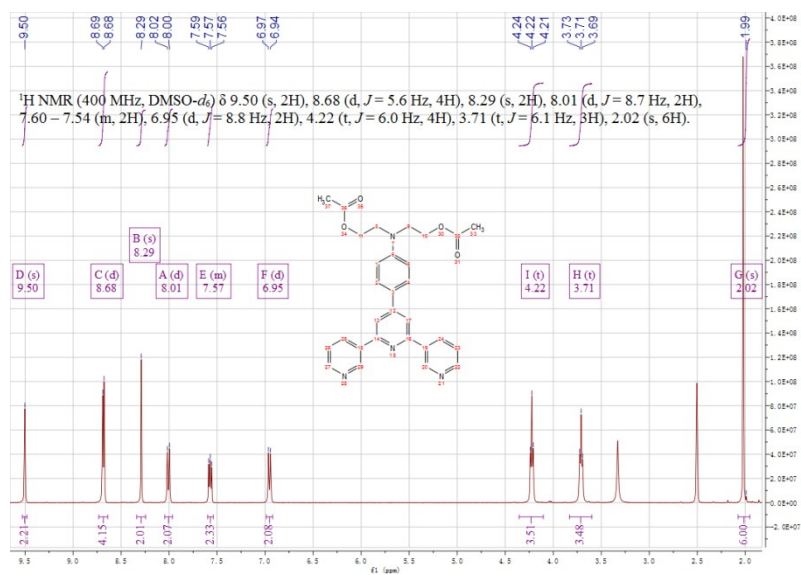
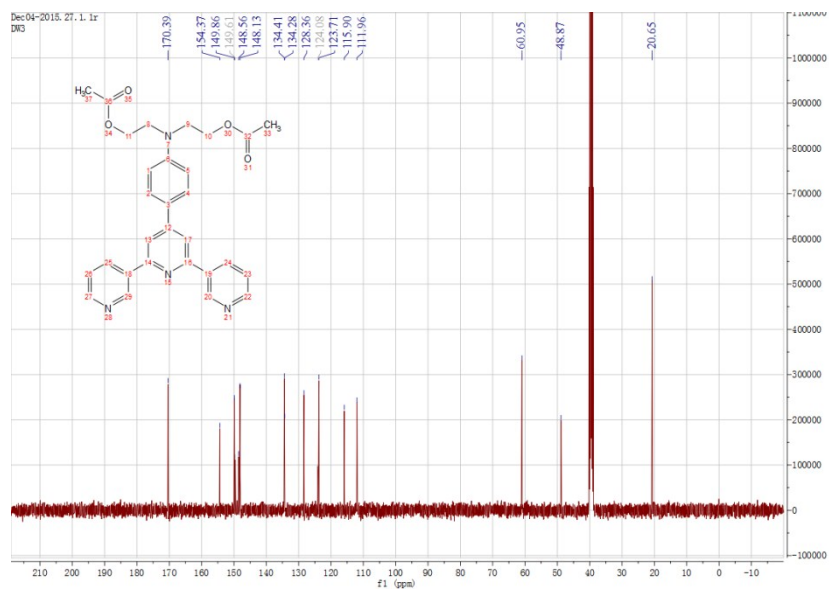
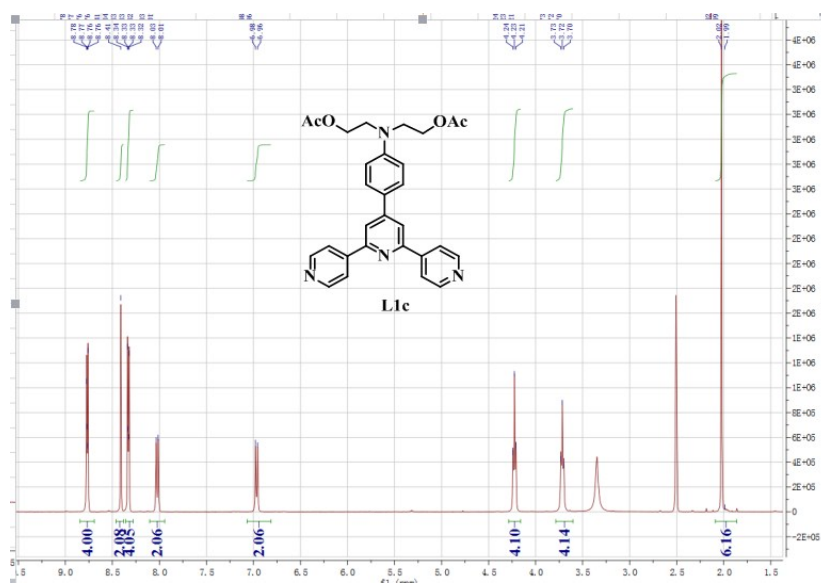


Fig. S3  $^1\text{H-NMR}$  spectrum of L1b.



**Fig. S4**  $^{13}\text{C}$ -NMR spectrum of **L1b**.



**Fig. S5**  $^1\text{H}$ -NMR spectrum of **L1c**.

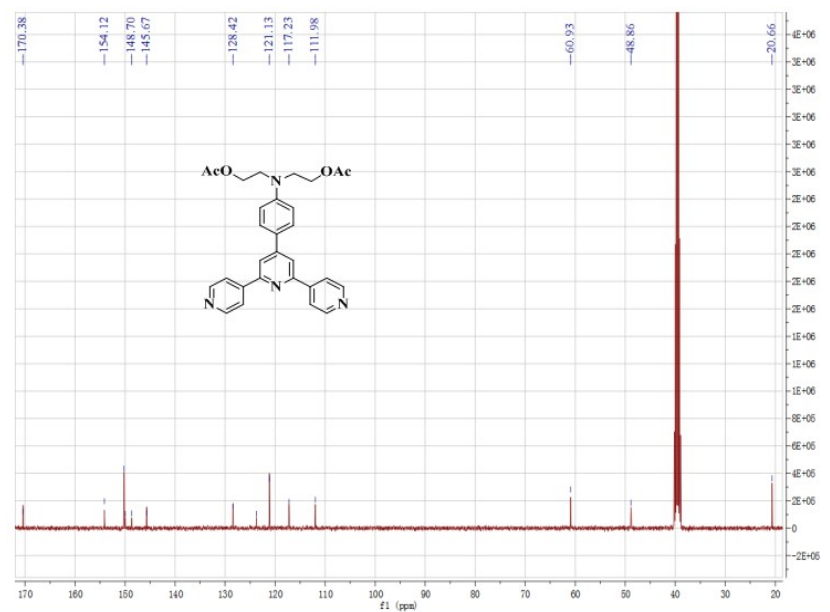


Fig. S6 <sup>13</sup>C-NMR spectrum of L1c.

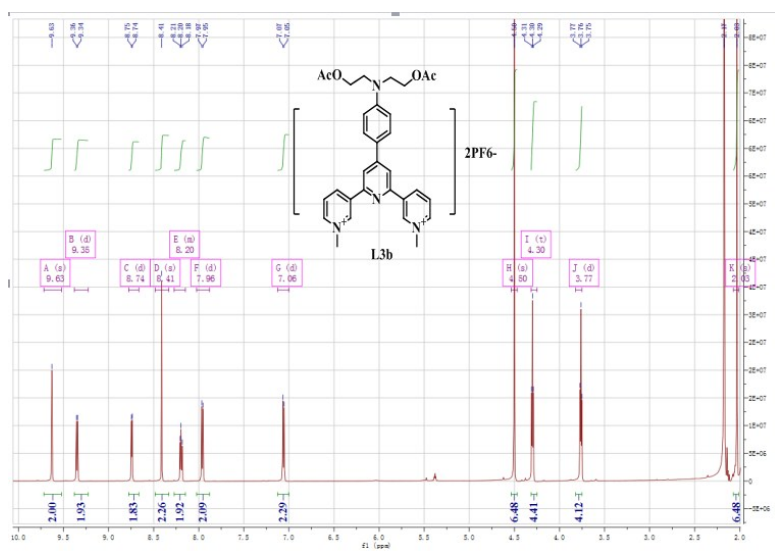


Fig. S7 <sup>1</sup>H-NMR spectrum of L2b.

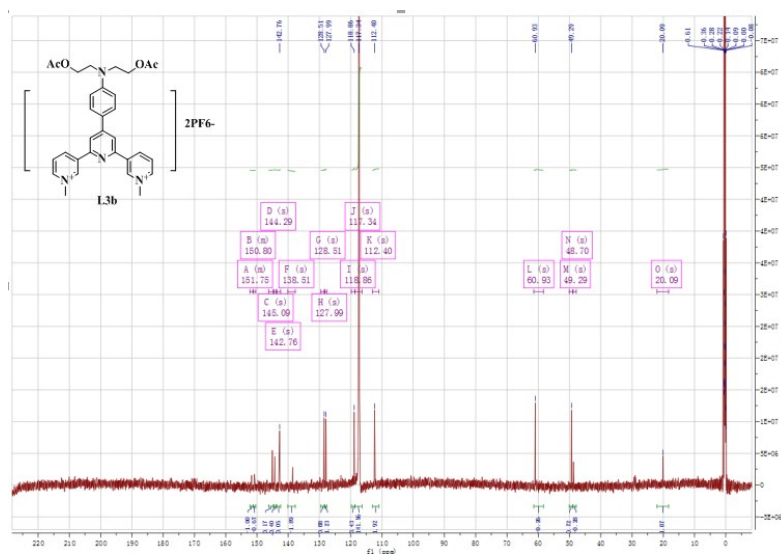


Fig. S8  $^{13}\text{C}$ -NMR spectrum of L2b.

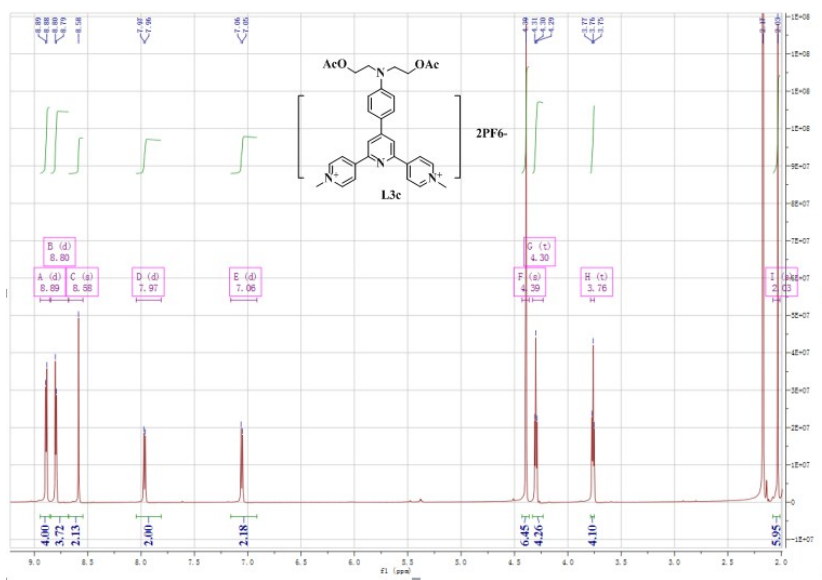


Fig. S9  $^1\text{H}$ -NMR spectrum of L2c.

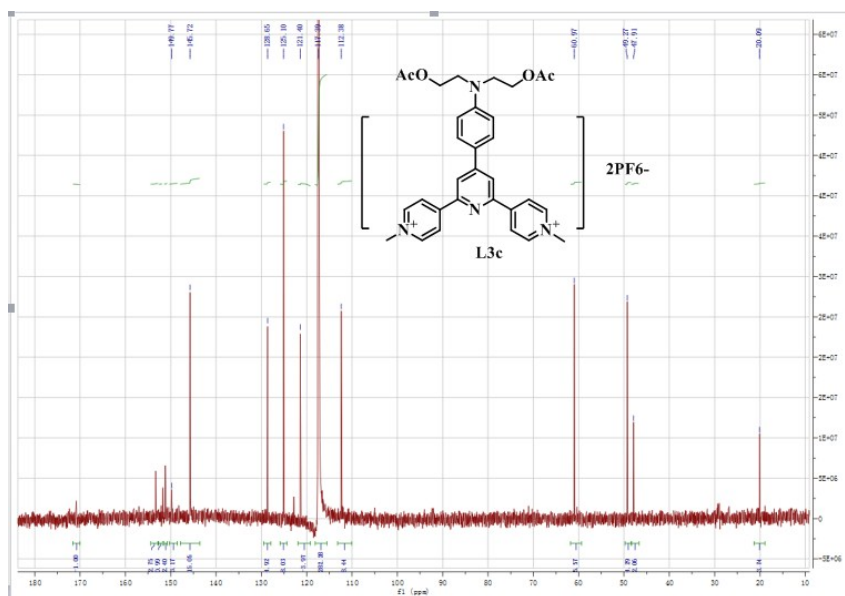


Fig. S10  $^{13}\text{C}$ -NMR spectrum of L2c.

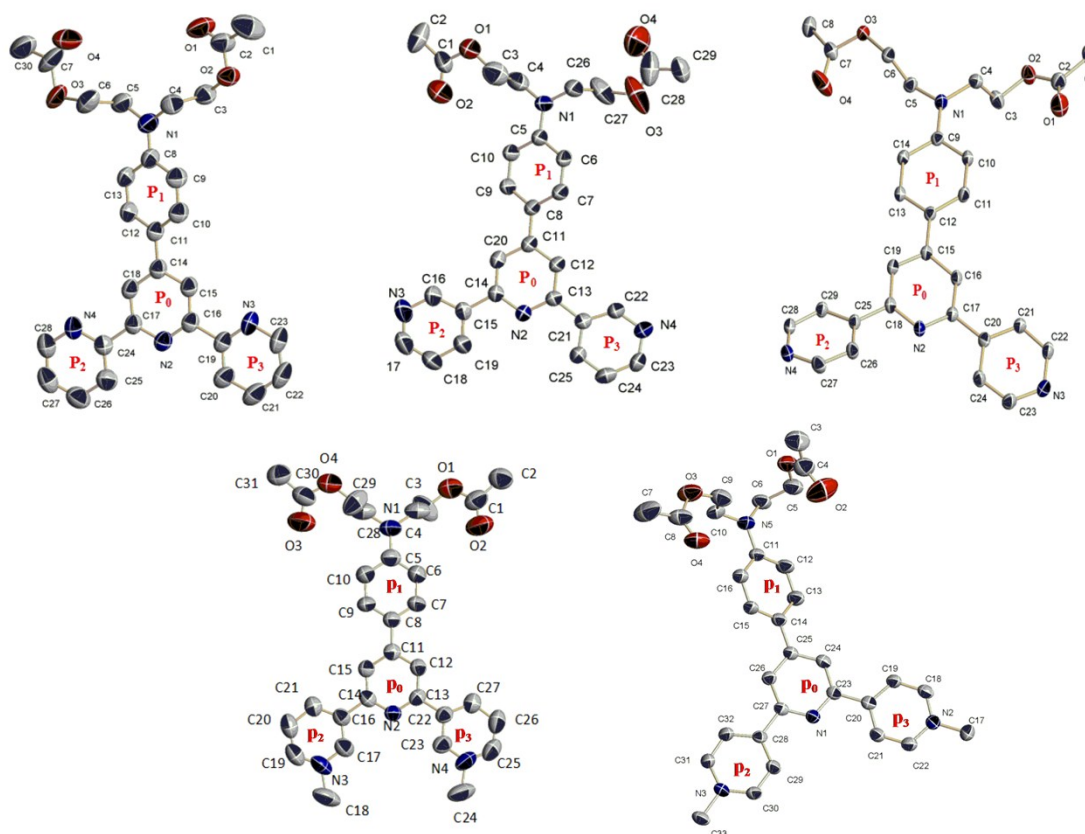
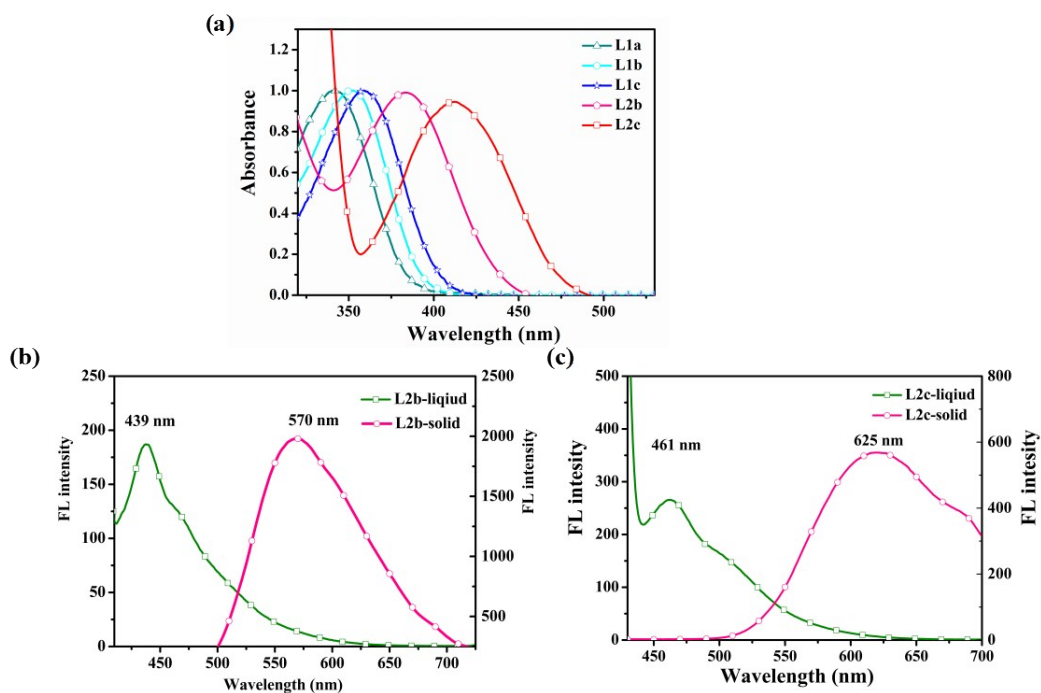
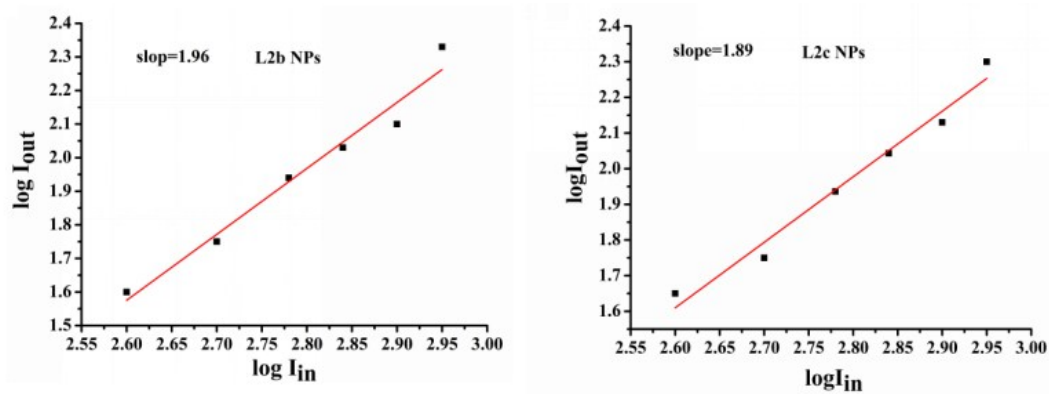


Fig. S11 The ORTEP structures of L1a, L1b, L1c, L2b and L2c.



**Fig. S12** UV-*vis* absorption spectra and fluorescence emission spectra of **L1** and **L2**. fluorescence emission spectra of **L2b**, **L2c** in solution state ( $c=10 \mu\text{M}$ ) and solid state (a, b, c).



**Fig. S13** Output fluorescence ( $I_{\text{out}}$ ) vs. the square of input laser power ( $I_{\text{in}}$ ) for **L2b** NPs and **L2c** NPs.

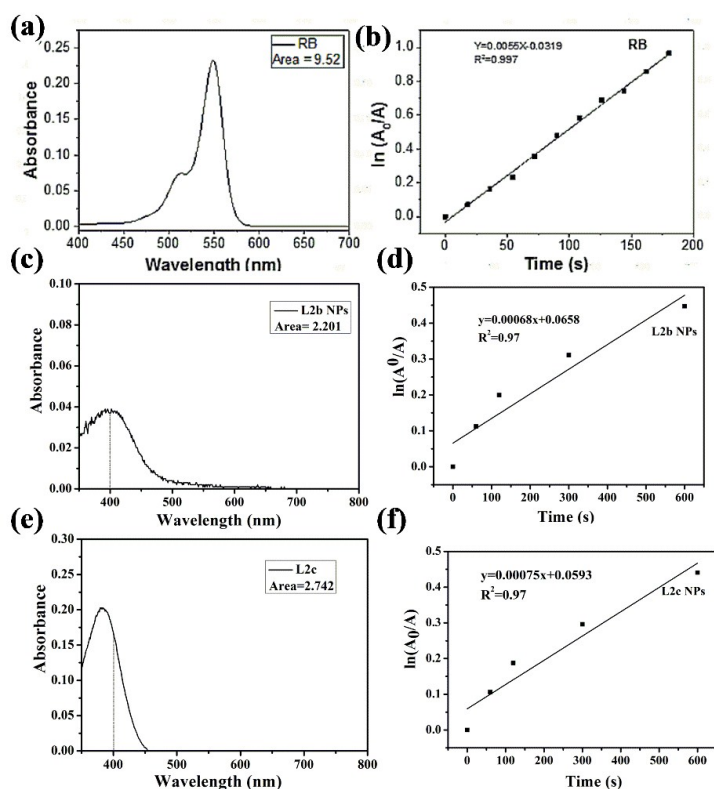


**Fig. S14** Chemical trapping measurements of the  $^1\text{O}_2$  quantum yield. The absorption peak area of RB (a); The decomposition rate constants of ADPA by RB (b); The absorption peak area of **L2b NPs** (c); The decomposition rate constants of ADPA by **L2b NPs** (d); The absorption peak area of **L2c NPs** (e); The decomposition rate constants of ADPA by **L2c NPs** (f).

**Table S1** Fluorescence quantum yield **L2b**, **L2c**, **L2b NPs** and **L2c NPs**.

Molecularly state	<b>L2b</b> 0.87 %	<b>L2c</b> 1.02 %
Aggregation state	<b>L2b NPs</b> 1.26 %	<b>L2c NPs</b> 2.17 %

**Table S2** Crystal data and structure refinement for **L1a**, **L1b**, **L1c**, **L2b** and **L2c**.

Compounds	<b>L1a</b>	<b>L1b</b>	<b>L1c</b>
Empirical	$\text{C}_{29}\text{H}_{28}\text{N}_4\text{O}_4$	$\text{C}_{29}\text{H}_{28}\text{N}_4\text{O}_4$	$\text{C}_{29}\text{H}_{28}\text{N}_4\text{O}_4$
Formula weight	496.55	496.55	496.55

Crystal system	Monoclinic	Monoclinic	Triclinic
Space group	P2 <sub>1</sub> /c	P2 <sub>1</sub> /c	P $\bar{1}$
<i>a</i> (Å)	14.6098(16)	22.944(3)	9.9838(9)
<i>b</i> (Å)	8.5527(9))	22.210(3)	11.1579(10)
<i>c</i> (Å)	22.221(2)	10.0282(14)	13.2772(12)
<i>a</i> [°]	90	90	96.2600(10)
<i>b</i> [°]	107.9420(10)	91.284(2)	105.2540(10)
<i>γ</i> [°]	90	90	115.5130(10)
<i>V</i> (Å <sup>3</sup> )	2641.5(5)	5109.0(12)	1245.10(19)
<i>Z</i>	4	4	2
<i>R</i> <sub>1</sub> , <i>wR</i> <sub>2</sub> [ <i>I</i> ≥ 2σ( <i>I</i> )]	0.0483, 0.1409	0.0679, 0.2103	0.0398, 0.0980
<i>R</i> <sub>1</sub> , <i>wR</i> <sub>2</sub> [ <i>all data</i> ]	0.0788, 0.1562	0.1892, 0.2467	0.0464, 0.1036
S on <i>F</i> <sup>2</sup>	1.058	1.032	0.990

Compounds	L2b	L2c
Empirical	C <sub>128</sub> H <sub>136</sub> F <sub>48</sub> N <sub>12</sub> O <sub>16</sub> P <sub>8</sub>	C <sub>32</sub> H <sub>34</sub> I <sub>2</sub> N <sub>4</sub> O <sub>4</sub>
Formula weight	3258.24	1435.67
Crystal system	monoclinic	triclinic
Space group	C2/c	P-1
<i>a</i> (Å)	19.940(10)	7.7972(9)
<i>b</i> (Å)	21.080(11)	13.3272(16)
<i>c</i> (Å)	8.921(5)	17.392(2)
<i>a</i> [°]	90	107.8110(10)
<i>β</i> [°]	104.143(8)	98.5610(10)
<i>γ</i> [°]	90	100.426(2)
<i>V</i> (Å <sup>3</sup> )	3636(3)	1651.5(3)
<i>Z</i>	1	1
<i>R</i> <sub>1</sub> , <i>wR</i> <sub>2</sub> [ <i>I</i> ≥ 2σ( <i>I</i> )]	0.1000, 0.2738	0.0400, 0.0855

$R_1, wR_2$ [all data]	0.1946, 0.3297	0.0597, 0.0950
S on $F^2$	0.965	1.041

**Table S3** Selected bond lengths (Å) and angles (°) for the crystal structure of **L1a**,  
**L1b**, **L1c**, **L2b** and **L2c**.

<b>L1a</b>	Dist.	<b>L1b</b>	Dist	<b>L1c</b>	Dist.
C2-C1	1.485(3)	C1-C2	1.450(6)	C1-C2	1.497(2)
C2-O1	1.193(2)	C1-O2	1.226(5)	C2-O1	1.198(2)
C2-O2	1.334(2)	O1-C1	1.294(5)	C2-O2	1.345(2)
C3-O2	1.429(2)	O1-C3	1.563(6)	C3-O2	1.446(19)
C3-C4	1.505(3)	C3-C4	1.421(6)	C3-C4	1.517(2)
C4-N1	1.452(2)	N1-C4	1.511(5)	C4-N1	1.456(19)
N1-C8	1.381(2)	N1-C5	1.381(4)	N1-C9	1.388(18)
C11-C14	1.475(2)	C8-C11	1.463(4)	C12-C15	1.478(2)
	Angle(°)		Angle(°)		Angle(°)
C1-C2-O1	126.00(2)	C2-C2-O1	113.8(5)	N3-C16-C17	125.7(17)
C1-C2-O2	113.30(2)	C2-C1-O2	124.3(5)	N3-C16-C14	122.9(16)
O2-C3-C4	110.58(16)	O1-C3-C4	101.7(4)	N3-C20-C19	177.0(13)
C4-N1-C8	121.60(16)	C3-C4-N1	104.8(5)	N4-C25-C24	179.2(14)
C10-C11-C14	161.49(18)	C7-C8-C11	122.3(3)	N1-C3-C4	164.08(14)
C15-C16-C19	176.58(14)	C12-C13-C21	122.1(3)	N1-C1-C2	170.8(15)
C18-C17-C24	174.49(17)	C20-C14-C15	122.4(3)	N1-C5-C10	121.7(13)

<b>L2b</b>	Dist.	<b>L2b</b>	Dist
C2-C1	1.528(3)	C4-O2	1.217(6)
C1-O1	1.300(2)	C4-O1	1.336(6)
C3-C4	1.468(2)	O1-C5	1.436(5)
C4-N1	1.490(2)	N5-C6	1.463(5)
N1-C5	1.347(3)	C11-N5	1.391(5)
C8-C11	1.488(2)	C14-C25	1.477(5)
C13-C22	1.478(2)	C23-C20	1.484(5)

N4-C24	1.488(4)	C17-N2	1.482(4)
	Angle(°)		Angle(°)
C2-C1-O2	124.15(2)	O1-C4-O2	120.9(5)
O1-C1-O2	123.37(2)	O1-C5-C6	110.8(4)
C4-N1-C5	121.95(16)	C6-N5-C11	121.1(3)
C7-C8-C11	121.79(16)	O3-C8-O4	122.3(5)
C8-C11-C12	122.00(18)	O3-C9-C10	109.8(4)
C12-C13-C22	122.54(14)	C10-N5-C11	119.6(3)
C25-N4-C24	121.42(17)	N1-C23-C20	115.0(3)

---

### Notes and references

- S1. Y. Hong, J. W. Y. Lam and B. Z. Tang, *Chem. Soc. Rev.*, 2011, **40**, 5361–5388.
- S2. C. D. Sherrill, T. Takatani and E. G. Hohenstein, *J. Phys. Chem. A*, 2009, **113**, 10146-10159.
- S3. K. Garg, E. Ganapathi, P. Rajakannu and M. Ravikanth, *Phys. Chem. Chem. Phys.*, 2015, **17**, 19465-19473.
- S4. T. Stubhan, T. Ameri, M. Salinas, J. Krantz, F. Machui, M. Halik and C. J. Brabec, *Appl. Phys. Lett.*, 2011, **98**, 122.
- S5. L. Zong, Y. Xie, C. Wang, J. R. Li, Q. Li and Z. Li, *Chem. Commun.*, 2016, **52**, 11496-11499.
- S6. Y. Yuan, C. J. Zhang, M. Gao, R. Zhang, B. Z. Tang and B. Liu, *Angew. Chem. Int. Ed.*, 2015, **54**, 1780-1786.
- S7. G. Feng, Y. Yuan, H. Fang, R. Zhang, B. Xing, G. Zhang and B. Liu, *Chem. Commun.*, 2015, **51**, 12490-12493.
- S8. C. J. Zhang, Q. Hu, G. Feng, R. Zhang, Y. Yuan, X. Lu and B. Liu, *Chem. Sci.*, 2015, **6**, 4580-4586.